The Astrophysical Journal, 817:114 (13pp), 2016 February 1 doi:10.3847/0004-637X/817/2/114

A LUMINOUS PECULIAR TYPE IA SUPERNOVA SN 2011HR: MORE LIKE SN 1991T OR SN 2007if?

Ju-Jia Zhang[1,2,3], Xiao-Feng Wang[3], Michele Sasdelli[4,5], Tian-Meng Zhang[6], Zheng-Wei Liu[7], Paolo A. Mazzali[4,5], Xiang-Cun Meng[1,2], Keiichi Maeda[8,9], Jun-Cheng Chen[3], Fang Huang[3], Xu-Lin Zhao[3], Kai-Cheng Zhang[3], Qian Zhai[1,2,10], Elena Pian[11,12], Bo Wang[1,2], Liang Chang[1,2], Wei-Min Yi[1,2], Chuan-Jun Wang[1,2,10], Xue-Li Wang[1,2], Yu-Xin Xin[1,2], Jian-Guo Wang[1,2], Bao-Li Lun[1,2], Xiang-Ming Zheng[1,2], Xi-Liang Zhang[1,2], Yu-Feng Fan[1,2], and Jin-Ming Bai[1,2]

[1] Yunnan Observatories (YNAO), Chinese Academy of Sciences, Kunming 650011, China; jujia@ynao.ac.cn
[2] Key Laboratory for the Structure and Evolution of Celestial Objects, Chinese Academy of Sciences, Kunming 650011, China
[3] Physics Department and Tsinghua Center for Astrophysics (THCA), Tsinghua University, Beijing 100084, China; wang_xf@mail.tsinghua.edu.cn
[4] Astrophysics Research Institute, Liverpool John Moores University, Liverpool Science Park, 146 Brownlow Hill, Liverpool L3 5RF, UK
[5] Max-Planck Institute fur Astrophysics, D-85748 Garching, Germany
[6] National Astronomical Observatories of China (NAOC), Chinese Academy of Sciences, Beijing 100012, China
[7] Argelander-Institut für Astronomie, Auf dem Hügel 71, D-53121, Bonn, Germany
[8] Department of Astronomy, Kyoto University, Kyoto, 606-8502, Japan
[9] Kavli Institute for the Physics and Mathematics of the Universe (WPI), University of Tokyo, 5-1-5 Kashiwanoha, Kashiwa, Chiba 277-8583, Japan
[10] University of Chinese Academy of Sciences, Chinese Academy of Sciences, Beijing 100049, China
[11] INAF-IASF-Bo, via Gobetti, 101, I-40129 Bologna, Italy
[12] Scuola Normale Superiore, Piazza dei Cavalieri 7, I-56126 Pisa, Italy
Received 2015 September 8; accepted 2015 December 12; published 2016 January 26

ABSTRACT

Photometric and spectroscopic observations of a slowly declining, luminous Type Ia supernova (SN Ia) SN 2011hr in the starburst galaxy NGC 2691 are presented. SN 2011hr is found to peak at $M_B = -19.84 \pm 0.40$ mag, with a postmaximum decline rate $\Delta m_{15}(B) = 0.92 \pm 0.03$ mag. From the maximum-light bolometric luminosity, $L = (2.30 \pm 0.90) \times 10^{43}$ erg s^{-1}, we estimate the mass of synthesized ^{56}Ni in SN 2011hr to be $M(^{56}\mathrm{Ni}) = 1.11 \pm 0.43\ M_{\odot}$. SN 2011hr appears more luminous than SN 1991T at around maximum light, and the absorption features from its intermediate-mass elements (IMEs) are noticeably weaker than those of the latter at similar phases. Spectral modeling suggests that SN 2011hr has IMEs of $\sim$0.07 $M_{\odot}$ in the outer ejecta, which is much lower than the typical value of normal SNe Ia (i.e., 0.3–0.4 $M_{\odot}$) and is also lower than the value of SN 1991T (i.e., $\sim$0.18 $M_{\odot}$). These results indicate that SN 2011hr may arise from a Chandrasekhar-mass white dwarf progenitor that experienced a more efficient burning process in the explosion. Nevertheless, it is still possible that SN 2011hr may serve as a transitional object connecting the SN 1991T-like SNe Ia with a superluminous subclass like SN 2007if given that the latter also shows very weak IMEs at all phases.

Key words: galaxies: individual (NGC 2691) – supernovae: general – supernovae: individual (SN 2011hr, SN 1991T, SN 2007if)

1. INTRODUCTION

Type Ia supernovae (SNe Ia), one of the most luminous stellar explosions, could explode within a similar mechanism: complete explosive destruction of a carbon–oxygen white dwarf (C–O WD) reaching the Chandrasekhar-mass limit (i.e., $\sim$1.4 $M_{\odot}$ for the C–O WD without rotation), most likely via accretion in a binary system, although other channels have been proposed (see, e.g., the review by Maoz et al. 2014). They show strikingly similar photometric and spectroscopic behavior in the optical (i.e., Suntzeff 1996; Filippenko 1997), and the remaining scatter can be better understood in terms of an empirical relation between light-curve width (i.e., $\Delta m_{15}(B)$) and luminosity (i.e., width–luminosity relation [WLR]; Phillips 1993). Based on that relation, SNe Ia have been successfully applied as luminosity distance indicators for measuring the expansion history of the universe (Riess et al. 1998; Schmidt et al. 1998; Perlmutter et al. 1999).

Observationally, SNe Ia could be divided into several different subclasses according to their spectral characteristics (Benetti 2005; Branch et al. 2009; Wang et al. 2009a). For example, SN 1991T (Filippenko et al. 1992b; Phillips et al. 1992) is spectroscopically different from the bulk of SNe Ia, lying at the luminous end of luminosity distribution. Its featureless spectra at early phase are characterized by appearances of strong Fe III lines and weak or absent lines of intermediate-mass elements (IMEs; e.g., Si II, S II, and Ca II), which are usually strong in the spectra of normal SNe Ia. It had a slowly declining light curve (e.g., $\Delta m_{15}(B) = 0.94$; Lira et al. 1998) and is $\sim$0.6 mag more luminous than normal ones (Filippenko et al. 1992b). However, Gibson & Stetson (2001) suggested that SN 1991T is indistinguishable from normal SNe Ia in luminosity. Altavilla et al. (2004) also showed that SN 1991T fits in the WLR and that its peculiarities are only spectroscopic. Through modeling of a series of early spectra, Mazzali et al. (1995) found that the absence of Fe II, Si II, and Ca II lines and the presence of strong Fe III lines are due to the low abundance of IMEs and the high ionization caused by the high luminosity. Superluminous SNe Ia such as SN 2003fg (Howell et al. 2006), SN 2006gz (Hichen et al. 2007), SN 2007if (Scalzo et al. 2010), and SN 2009dc (Taubenberger et al. 2010; Silverman et al. 2011; Hachinger et al. 2012) are called super-Chandrasekhar (SC) SN Ia candidates. These SNe Ia are required to have progenitor masses exceeding the Chandrasekhar-mass limit if their luminosities are entirely attributed to the radioactive decay of ^{56}Ni.

In this paper, we present observations of SN 2011hr (R. A. $= 08^{h}54^{m}46^{s}.03$, decl. $= +39°32'16''.1$), which was

discovered on UT 2011 November 8.54 (UT time is used throughout this paper) by the Katzman Automatic Imaging Telescope, Lick Observatory, USA (Nayak et al. 2011). The supernova is located 3.″4 west and 3.″7 north of the center of NGC 2691, which is equivalent to a projected distance ~1.5 kpc using the distance of the host adopted in this paper (i.e., $D \approx 60.0$ Mpc). Two days after the discovery, an optical spectrum was taken with the Li-Jiang 2.4 m telescope (hereafter LJT) of Yunnan observatories (YNAO), China, showing that it was a young SN 1991T-like SN Ia at about 10 days before maximum light, with prominent iron lines in the spectrum (Zhang et al. 2011). A follow-up photometric and spectroscopic observing campaign was immediately established for SN 2011hr.

This paper is organized as follows. Photometric observations and data reductions are described in Section 2, where the light and color curves are investigated. Section 3 presents the spectroscopic observations. In Section 4 we derive the bolometric luminosity and the mass of ^{56}Ni synthesized in the explosion, and we model the early-time spectra using abundance tomography. Moreover, a possible explosion mechanism is also discussed in this section. A brief summary is given in Section 5.

2. PHOTOMETRY

2.1. Observations and Data Reduction

The photometric observations of SN 2011hr were performed in broad *UBVRI* bands with the Tsinghua-NAOC 0.8 m telescope (hereafter TNT; Wang et al. 2008; Huang et al. 2012) at Xing-Long Observatory of NAOC. This telescope is equipped with a 1340 × 1300 CCD (PI VersArray: 1300B), providing a field of view (FOV) of 11.′5 × 11.′2 with a spatial resolution of ~0.″52 pixel^{-1}. The typical exposure times are 180 s in the *BVRI* bands and 300 s in the *U* band when taking images of SN 2011hr. These images have typical FWHM of about 2.″5. The CCD images were reduced using standard IRAF routines. The data collections started from $t \approx -14$ days and lasted until $t \approx +70$ days relative to the *B*-band maximum light. All CCD images were reduced using the IRAF[13] standard procedure.

Since SN 2011hr exploded near the center of its host galaxy, the step of subtracting the galaxy template from the SN images is necessary for accurate photometry, in particular when the SN became faint and/or the images were taken under poor seeing conditions. Higher-quality template images were obtained with the TNT on 2013 May 11, when the SN was sufficiently faint. Using the galaxy-subtracted images, we measured the instrumental magnitudes of the SN and the local standard stars (labeled in Figure 1) by aperture photometry, performed using the IRAF DAOPHOT package (Stetson 1987). The radius for the photometric aperture is set as 2.0 times the FWHM; the sky background light was determined from the median counts at a radius that is 5.0 times the FWHM. Twelve local standard stars in the field of SN 2011hr are labeled in Figure 1. We transformed the instrumental magnitudes of these reference stars to the standard Johnson *UBV* (Johnson et al. 1966) and Kron–Cousins *RI* (Cousins 1981) systems through the following transforming equations (Huang et al. 2012):

$$U = u + 0.22(U - B), \quad (1)$$

$$B = b + 0.15(B - V), \quad (2)$$

$$V = v - 0.06(B - V), \quad (3)$$

$$R = r - 0.10(V - R), \quad (4)$$

$$I = i + 0.02(V - I), \quad (5)$$

where *UBVRI* represent the magnitudes in the standard system and *ubvri* represent the instrumental magnitudes. The color term coefficient was determined by observing Landolt (1992) standards on photometric nights. The magnitudes of these reference stars are listed in Table 1, and they are then used to convert the photometry of SN 2011hr to the standard *UBVRI* magnitudes as shown in Table 2.

2.2. Light Curves

Figure 2 displays the *UBVRI*-band light curves of SN 2011hr (see details in Table 2). Some basic photometric parameters such as the maximum-light dates, peak magnitudes, and magnitude decline rates (Δm_{15}; Phillips 1993) can be derived from a polynomial fit to the observed light curves, which are listed in Table 3. We find that SN 2011hr reached a *B*-band maximum brightness of 14.95 ± 0.03 mag on JD $2{,}455{,}889.62 \pm 0.30$ (2011 November 23.12), with a decline rate $\Delta m_{15}(B) = 0.92 \pm 0.03$ mag. The slower decline rate suggests that SN 2011hr should be intrinsically luminous if it follows the WLR (e.g., Phillips 1993; Riess et al. 1996; Goldhaber et al. 2001; Guy et al. 2005); see also Table 3 and detailed discussion in Section 2.5. After correcting for a Galactic reddening of $E(B - V) = 0.02$ mag (Schlegel et al. 1998), the color index $B_{\max} - V_{\max}$ becomes 0.23 ± 0.04 mag. On the other hand, the corresponding color index is about 0.13 ± 0.03 mag for SN 1991T. This suggests that both SN 2011hr and SN 1991T suffer a significant host-galaxy reddening assuming that their intrinsic colors are comparable to that established for normal SNe Ia (e.g., Phillips et al. 1999; Wang et al. 2009b); see also Sections 2.3 and 2.4.

Overplotted in Figure 2 are the light curves of other well-observed SNe, including overluminous SN Ia SN 1991T ($\Delta m_{15} = 0.94$ mag; Sasdelli et al. 2014 and therein), SN 1999aa ($\Delta m_{15}(B) = 0.83$ mag; Jha et al. 2006), the "golden standard" SN Ia SN 2005cf ($\Delta m_{15}(B) = 1.05$ mag; Wang et al. 2009b), the superluminous SN 2007if ($\Delta m_{15}(B) = 0.71$; Scalzo et al. 2010) and SN 2009dc ($\Delta m_{15}(B) = 0.71$; Taubenberger et al. 2010). In general, SN 2011hr shows a close resemblance to SN 1991T in *UBVRI*-band photometry. Compared to SN 2011hr/SN 1991T, the superluminous object SN 2009dc shows apparently broader light curves, especially in the redder bands, where its secondary maximum/shoulder feature is more prominent. Note that another so-called superluminous SN Ia, SN 2007if, is found to be more similar in morphology to SN 2011hr/SN 1991T.

2.3. Color Curves

Figure 3 shows the color curves of SN 2011hr. Overplotted are the color curves of SN 1991T, SN 1999aa, SN 2005cf, SN 2007if, and SN 2009dc. All of these color curves (including those of SN 2011hr) are corrected for the reddening of the Milky Way and the host galaxy. The reddening of SN 2011hr is discussed in the following section.

[13] IRAF, the Image Reduction and Analysis Facility, is distributed by the National Optical Astronomy Observatory, which is operated by the Association of Universities for Research in Astronomy (AURA), Inc., under cooperative agreement with the National Science Foundation (NSF).

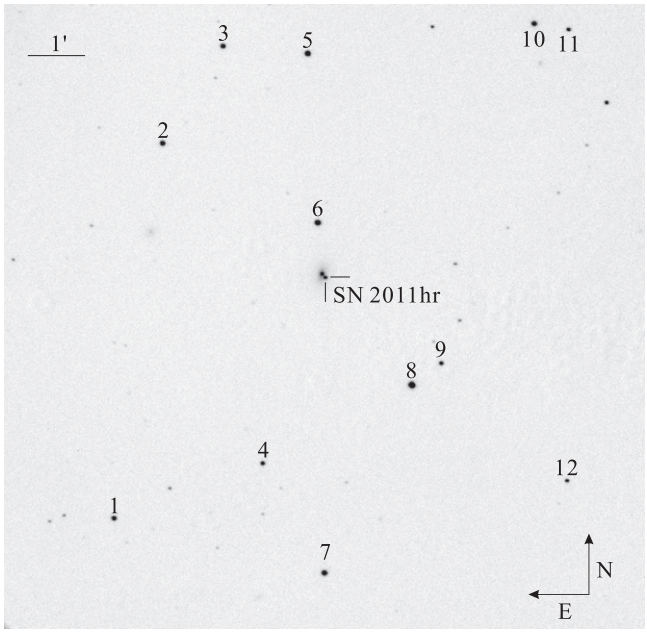

Figure 1. *R*-band image of SN 2011hr, which was taken on 2011 November 14.81 with the Tsinghua-NAOC 0.8 m telescope. The mean FWHM of this image is 2.″60 under the scale of 0.″52 pixel^{-1}. The supernova and reference stars are marked. North is up, and east is to the left.

Table 1
Magnitudes of the Photometric Standards in the Field of SN 2011hr

Star	*U*(mag)	*B*(mag)	*V*(mag)	*R*(mag)	*I*(mag)
1	16.01(03)	15.27(02)	14.50(03)	14.00(02)	13.66(02)
2	14.15(02)	14.15(02)	13.78(02)	13.48(02)	13.32(01)
3	17.03(04)	15.66(02)	14.58(03)	13.79(02)	13.33(01)
4	17.99(04)	16.61(03)	15.31(03)	14.39(02)	13.72(02)
5	16.06(03)	14.81(02)	13.88(02)	13.22(02)	12.88(01)
6	16.27(03)	14.96(03)	13.71(02)	12.99(02)	12.46(01)
7	14.36(03)	14.26(02)	13.67(02)	13.35(02)	13.17(02)
8	13.94(02)	13.47(01)	12.76(01)	12.40(01)	12.15(01)
9	15.91(03)	15.53(02)	14.91(03)	14.52(02)	14.26(02)
10	16.57(04)	15.67(03)	14.44(03)	13.48(03)	12.76(03)
11	17.30(05)	16.28(04)	15.38(04)	14.70(04)	14.39(04)
12	16.41(03)	16.13(02)	15.39(03)	14.96(03)	14.67(02)

Note. Uncertainties, in units of 0.01 mag, are 1σ. Figure 1 shows a finding chart of SN 2011hr and the comparison stars.

At early time, the $U-B$ colors of the luminous/super-luminous SNe Ia (including SN 2011hr) show distinct behavior compared to the normal SN 2005cf. The former group tends to become progressively redder after explosion, while SN 2005cf shows a "red–blue–red" evolutionary trend at a similar phase. At around maximum light, the $B-V$ color of SN 2011hr and SN 1991T is redder than that of other comparison SNe Ia. SN 2011hr and SN 1991T are also found to be redder by 0.1–0.2 mag than predicted by the Lira–Phillips relation (Phillips et al. 1999; see solid line in Figure 3). Among our comparison sample, SN 2009dc shows the bluest $U-B$ and $B-V$ colors at $t<+35$ days, while it (and SN 2007if) shows redder $V-R$ and $V-I$ colors. Large scatter can be seen in the $V-I$ color, where the strength of the Ca II near-IR (NIR) triplet could have a dominant effect. In general, SN 2011hr shows a color evolution that is quite similar to that of SN 1991T and SN 2007if at all phases.

2.4. Extinction

The Milky Way reddening of SN 2011hr is $E(B-V)_{\rm Gal}=0.02$ mag (Schlegel et al. 1998), corresponding to an extinction of 0.06 mag adopting the standard Galactic reddening law (i.e., $R_V=3.1$; Cardelli et al. 1989). The reddening due to the host galaxy can be estimated by several empirical methods. For instance, a comparison of the late-time $B-V$ color with that predicted by the Lira–Phillips relation (Phillips et al. 1999) gives a host-galaxy reddening of $E(B-V)_{\rm host}=0.29\pm0.07$ mag for SN 2011hr. The peak $B_{\rm max}-V_{\rm max}$ color has also been used as a better reddening indicator for SNe Ia (Phillips et al. 1999; Wang et al. 2009b), based on its dependence on $\Delta m_{15}(B)$. For SN 2011hr, the observed peak $B-V$ color is 0.23 ± 0.04 mag, which suggests a host-galaxy reddening of $E(B-V)=0.32\pm0.06$ mag. However, a scatter of about 0.1 mag might exist for the above estimates considering that such overluminous SNe Ia may have intrinsically different colors relative to the normal SNe Ia.

The low-resolution spectra of SN 2011hr show prominent signatures of Na I D absorption, for which the equivalent width (EW) of this absorption can be derived by using a double-Gaussian fit as shown in Figure 4. The best fit yields EW (Na I D) $=1.42\pm0.02$ Å with $\mathrm{EW_{D1}}=0.84\pm0.01$ Å and $\mathrm{EW_{D2}}=0.58\pm0.01$ Å. Based on an empirical correlation between reddening and the EW of Na I D, namely, $E(B-V)=0.16\,\mathrm{EW}-0.01$ [Å] (Turatto et al. 2003), we estimate $E(B-V)_{\rm host}$ to be 0.22 ± 0.10 mag for SN 2011hr, which is consistent with the result derived from the photometric $B-V$ color within 1σ error.

Combining the results from both photometry and Na I D absorption, a host-galaxy reddening of $E(B-V)_{\rm host}=0.25\pm0.10$ can be obtained for SN 2011hr. On the other hand, the spectral modeling presented in Section 4.3 suggests a moderate host-galaxy reddening, i.e., $E(B-V)_{\rm host}=0.15$ mag, which seems to be more reasonable as it matches the observed colors. Therefore, a mean value $E(B-V)_{\rm total}=0.22\pm0.05$ mag is adopted as the total reddening of SN 2011hr in this paper.

2.5. Distance

The actual luminosity of SN 2011hr is affected by the uncertainty in the distance to the SN. Table 4 lists the measurements obtained using different methods. One can see that these measurements show significant dispersion. For example, the distance derived from the redshift of the host galaxy NGC 2691 and the Hubble flow is 59.3 ± 4.0 Mpc (Mould et al. 2000), which agrees with the result from the Tully–Fisher relation (60.2 ± 10.0 Mpc; Theureau et al. 2007). These two values are larger than the luminosity distance derived for the SN using the original Phillips (1993) relation but close to that derived from the modified relation for 91T-like events in Blondin et al. (2012), as listed in Table 4.

On the other hand, we can also estimate the distance to SN 2011hr based on its NIR magnitude, since the *JHK*-band luminosities of SNe Ia are relatively insensitive to the reddening and are more uniform around the peak compared to the corresponding values in the optical bands (Meikle 2000; Krisciunas et al. 2004; Barone-Nugent et al. 2012). Additionally, some peculiar SNe Ia such as SN 1999aa, SN 1999ac, and SN 1999aw are found to have normal luminosities in the NIR bands (Krisciunas et al. 2004), though they appear somewhat

Table 2
The *UBV RI* Photometry of SN 2011hr

MJD	Epoch[a]	*U* (mag)	*B* (mag)	*V* (mag)	*R* (mag)	*I* (mag)
55,874.04	−15.08	⋯	⋯	⋯	16.90(20)	⋯
55,875.08	−14.04	⋯	⋯	⋯	17.10(20)	⋯
55,875.34	−13.78	16.17(08)	16.90(03)	16.71(02)	16.53(02)	16.43(02)
55,876.36	−12.76	⋯	16.47(02)	16.24(01)	15.98(02)	16.01(01)
55,878.32	−10.80	⋯	15.91(02)	15.71(04)	15.59(02)	15.41(01)
55,879.30	−9.82	15.00(05)	15.60(02)	15.38(02)	15.33(01)	15.24(01)
55,880.31	−8.81	14.89(05)	15.41(02)	15.22(01)	15.10(01)	15.15(03)
55,890.31	1.19	14.71(03)	14.97(02)	14.76(01)	14.63(01)	14.84(01)
55,892.31	3.19	14.82(03)	15.01(02)	14.73(01)	14.62(01)	14.83(01)
55,899.36	10.24	15.33(04)	15.40(02)	14.97(05)	14.93(01)	15.27(04)
55,904.33	15.21	16.03(08)	15.93(02)	15.26(01)	15.12(04)	15.24(03)
55,905.33	16.21	⋯	⋯	15.29(05)	15.18(04)	15.23(05)
55,906.31	17.19	16.28(05)	16.06(03)	15.36(02)	15.22(03)	15.28(01)
55,907.33	18.21	16.45(06)	16.18(04)	15.43(01)	15.32(01)	15.26(01)
55,910.35	21.23	⋯	⋯	15.54(04)	15.47(06)	15.24(05)
55,911.33	22.21	17.00(05)	16.69(02)	15.59(05)	15.51(04)	15.25(04)
55,912.33	23.21	17.07(05)	16.79(05)	15.63(01)	15.47(01)	15.19(03)
55,915.26	26.14	17.37(05)	17.01(03)	15.81(01)	15.43(01)	15.22(04)
55,916.31	27.19	17.38(05)	17.18(02)	15.84(05)	15.52(02)	15.26(02)
55,917.33	28.21	17.47(09)	17.18(02)	15.89(05)	15.59(01)	15.29(03)
55,918.31	29.19	17.54(06)	17.21(07)	15.94(01)	15.51(01)	15.26(04)
55,919.25	30.13	17.58(10)	17.31(02)	15.99(01)	15.51(01)	15.26(03)
55,920.39	31.27	17.61(05)	17.37(01)	16.06(05)	15.60(01)	15.29(02)
55,927.23	38.11	18.02(06)	17.65(07)	16.28(05)	15.93(05)	15.55(05)
55,929.24	40.12	18.13(06)	17.77(08)	16.42(05)	16.03(05)	15.64(06)
55,930.17	41.05	18.18(10)	17.78(04)	16.49(05)	16.11(04)	15.68(08)
55,931.21	42.09	18.20(09)	17.82(04)	16.53(04)	16.13(02)	15.78(02)
55,932.21	43.09	18.23(06)	17.88(05)	16.55(04)	16.23(01)	15.84(03)
55,935.19	46.07	18.26(07)	17.96(04)	16.69(04)	16.39(01)	16.04(02)
55,936.20	47.08	18.32(05)	17.88(03)	16.74(05)	16.42(04)	16.17(05)
55,937.11	47.99	⋯	⋯	⋯	16.48(03)	⋯
55,938.21	49.09	18.31(09)	17.92(04)	16.76(05)	16.51(05)	16.19(03)
55,939.25	50.13	18.34(10)	17.95(03)	16.82(04)	16.52(08)	16.35(02)
55,941.08	51.96	18.46(08)	18.01(03)	16.92(05)	16.55(03)	16.39(06)
55,954.12	65.00	18.56(10)	18.11(03)	17.21(02)	16.91(05)	16.87(05)
55,955.30	66.18	18.62(12)	18.12(07)	17.28(04)	17.04(05)	⋯
55,956.08	66.96	18.63(12)	18.19(08)	17.31(05)	17.08(05)	16.99(07)
55,958.06	68.94	⋯	⋯	17.34(07)	17.14(06)	⋯
55,959.10	69.98	⋯	18.27(08)	17.36(07)	17.21(08)	⋯

Note. Uncertainties, in units of 0.01 mag, are 1σ; MJD = JD − 2,400,000.5.
[a] Relative to the epoch of *B*-band maximum on 2011 November 23.49, JD 2,455,889.62.

peculiar in optical bands. Based on the NIR photometry of 13 SNe Ia (including SN 2011hr), Weyant et al. (2014) estimated their mean absolute peak magnitude as -18.31 ± 0.02 mag in the *H* band. Taking the observed *H*-band peak magnitude of 15.02 ± 0.20 mag for SN 2011hr (Weyant et al. 2014) and assuming that it has a similar absolute *H*-band magnitude, we get a distance modulus $m - M = 33.20 \pm 0.20$ mag or $D = 43.7 \pm 5.0$ Mpc. This estimate is much smaller than the Tully–Fisher distance and that inferred from the Hubble flow. Note, however, that the dispersion of the sample from Weyant et al. (2014) will decrease significantly from $\sigma_H = 0.23$ mag to ∼0.18 mag if SN 2011hr was excluded in the analysis. This is due to the fact that SN 2011hr is actually more luminous than normal SNe Ia by ∼0.7 mag in the *H* band.

As the distance derived from Hubble expansion is independent of corrections for reddening and agrees well with the estimate from the Tully–Fisher relation, a distance of $D = 60.0 \pm 6.0$ Mpc is thus adopted for SN 2011hr in this paper.

3. SPECTROSCOPY

3.1. Observations and Data Reduction

A journal of spectroscopic observation of SN 2011hr is given in Table 5. A total of 11 low-resolution spectra were obtained with the LJT, the Yunnan Faint Object Spectrograph and Camera (YFOSC; Zhang et al. 2014), the Xing-Long 2.16 m telescope (hereafter XLT), and the Beijing Faint Object Spectrograph and Camera (BFOSC). During our spectral observations, the typical FWHM was about 1.″5 at Lijiang Observatory and about 2.″5 at Xinglong Observatory. All spectra were reduced using standard IRAF routines. Flux calibration was done using spectrophotometric flux standard stars observed at a similar airmass on the same night. The spectra were further corrected for the atmospheric absorption and telluric lines at the site. Synthetic photometry computed using Bessell (1992) passbands was introduced to check the spectroscopic flux calibration, while the spectral fluxes were

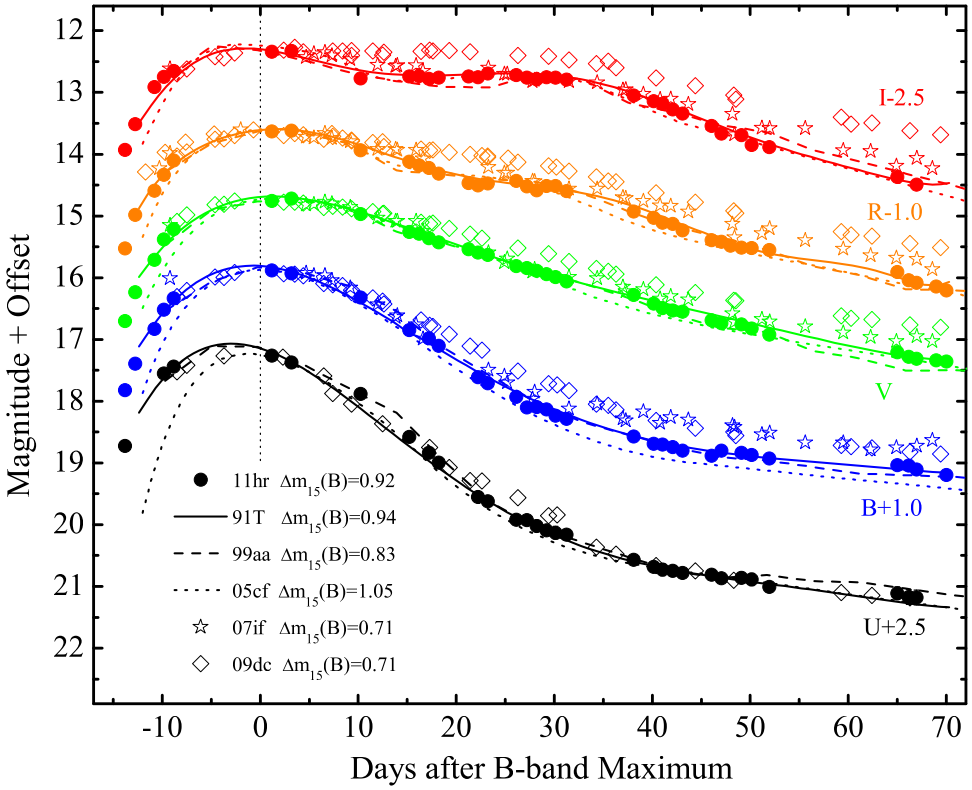

Figure 2. *UBVRI*-band light curves of SN 2011hr, compared with those of SN 1991T, SN 1999aa, SN 2005cf, SN 2007if, and SN 2009dc (see text for references). The light curves of SN 2011hr are shifted vertically by numbers as indicated in the plot, and those of the comparison SNe are normalized to the peak magnitudes of SN 2011hr. The light curves of SN 1991T, SN 1999aa, and SN 2005cf have been slightly smoothed with a low-order polynomial for a better display.

Table 3
Light-curve Parameters of SN 2011hr

Band	λ_{mid} (Å)	t_{max}[a] (−2455000.5)	m_{peak}[b] (mag)	Δm_{15}[b] (mag)	M_{peak}[b] (mag)
U	3650	887.39(50)	14.63(03)	1.04(05)	−20.34(45)
B	4450	889.12(30)	14.95(02)	0.92(03)	−19.84(40)
V	5500	889.95(30)	14.70(03)	0.59(03)	−19.87(35)
R	6450	890.01(30)	14.62(02)	0.53(05)	−19.81(30)
I	7870	890.10(40)	14.70(03)	0.45(05)	−19.57(30)

Notes.
[a] 1σ uncertainties, in units of 0.01 days.
[b] 1σ uncertainties, in units of 0.01 mag.

adjusted to match the contemporaneous photometry. Figure 4 shows the complete spectral evolution of SN 2011hr.

3.2. Temporal Evolution of the Spectra

The spectra of SN 2011hr are described in more detail and compared to those of SN 1991T, SN 1999aa, SN 2005cf, SN 2007if, and SN 2009dc at different epochs in this section; see Figures 5, 6, and 7. All of these spectra have been corrected for redshift and reddening. The line identifications labeled in these figures are based on the modeling results for SN 1991T (Mazzali et al. 1995). The spectra of SN 2011hr have been corrected for the contamination of host-galaxy emission lines by using the spectrum taken at the site of SN 2011hr (with the LJT and YFOSC) at ∼500 days after maximum light.

3.2.1. The Early Phase

Figure 5 displays the spectra at $t < -7$ days. At this phase, the spectra usually carry the signature of the ejecta materials in the outermost layers and show mainly lines of IMEs for normal SNe Ia. The spectra of SN 2011hr are rather similar to those of 91T-like events, which are characterized by a blue continuum and prominent Fe III/Fe II lines. Two main absorption features in SN 2011hr and SN 1991T are multiplets of Fe III or Fe II lines at 4404 and 5129 Å. By contrast, lines from IMEs (e.g., Si II, S II, and O I) are very weak, which is a common characteristic of 91T-like SNe Ia. Lines of Si III are also present in the spectra. This peculiar phenomenon is due to a combination of high photospheric temperature and low abundance of light elements in the ejecta (Mazzali et al. 1995; Sasdelli et al. 2014).

A notable difference between SN 2011hr and SN 1991T is the absorption near 3900 Å at $t \approx -10$ and -8 days. Such a feature could be a blend of Fe III λ4006 and Ni II λ4067. The spectrum of SN 1999aa at $t \approx -9$ days shows both strong Fe III lines and also a strong Ca II H&K feature, while the absorption of Si II λ6355 is weaker in this object. Spectral databases of SNe Ia (e.g., Blondin et al. 2012; Silverman et al. 2012) indicate that most SNe show strong Ca II absorption from very early phases to 4–5 months after explosion. However, as shown in Figure 8, the Ca II lines in the spectra of SN 2011hr are even weaker than those of SN 1991T at some phases after maximum light.

At $t < -7$ days, the spectrum of SN 2007if is also featureless and dominated by lines of doubly ionized Fe and Si. Ca II absorptions are also very weak at this phase. Note that the Fe III lines are weaker in SN 2007if compared to those in SN 2011hr at this phase. In SN 2007if, a weak absorption on

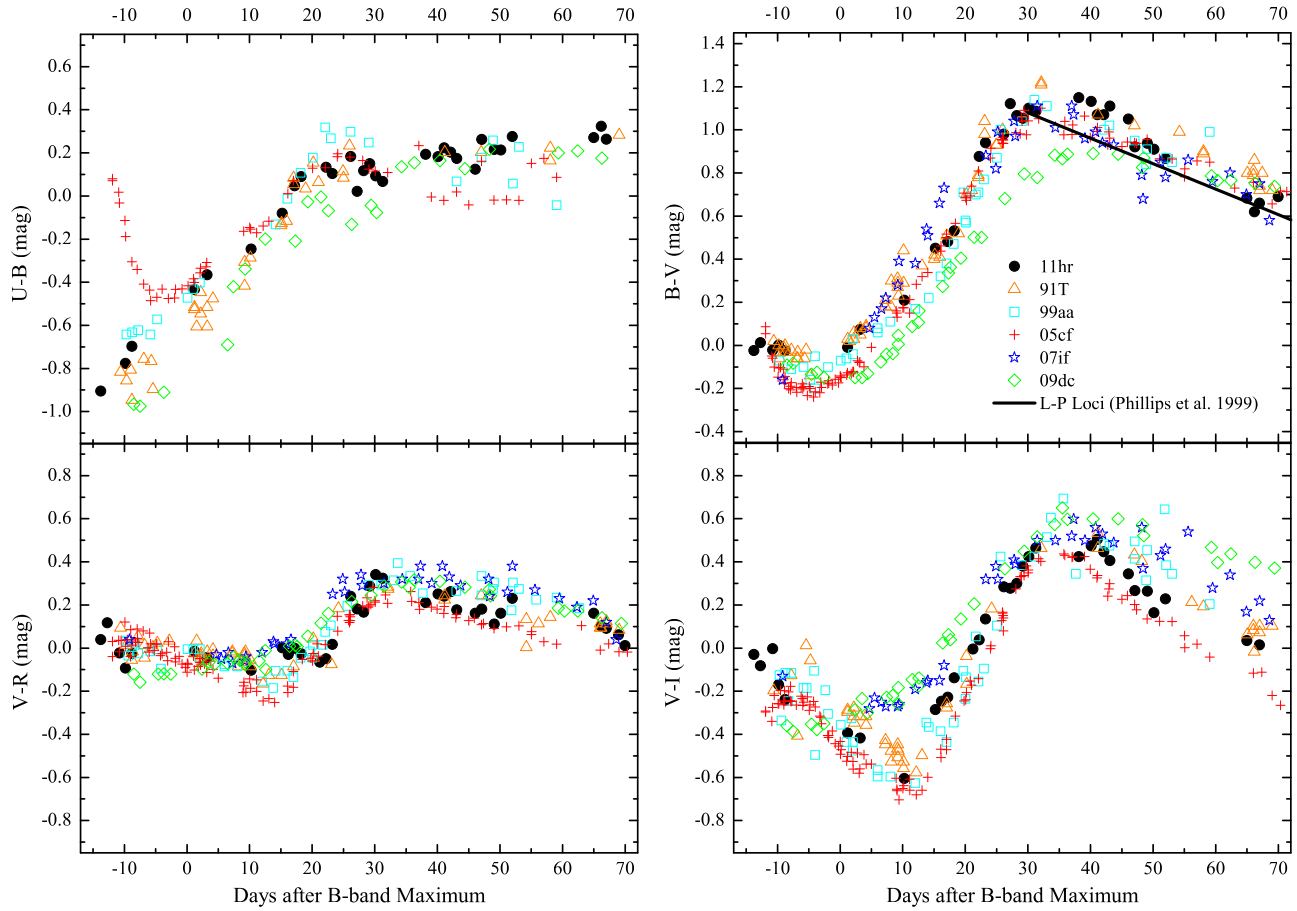

Figure 3. Optical color curves of SN 2011hr, in comparison with those of SN 1991T, SN 1999aa, SN 2005cf, SN 2007if, and SN 2009dc. See text for details.

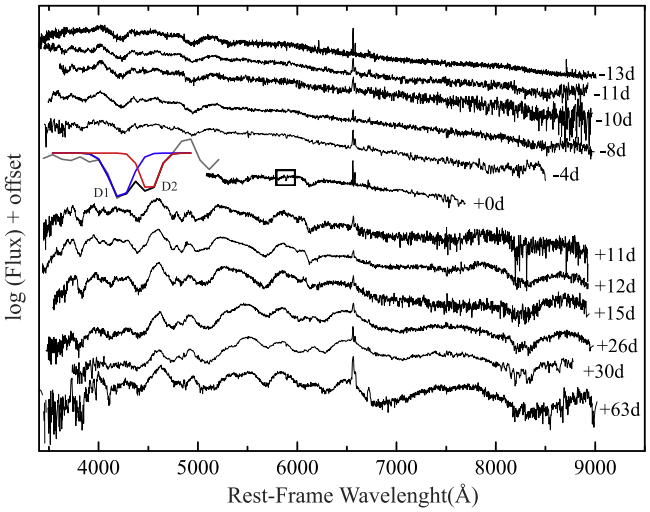

Figure 4. Optical spectral evolution of SN 2011hr. The spectra have been corrected for the redshift of the host galaxy ($v_{\rm hel} = 4137$ km s^{-1}) and telluric lines. They have been shifted vertically by arbitrary amounts for clarity. The numbers on the right-hand side mark the epochs of the spectra in days since the *B*-band maximum. The Na I D absorption of the host galaxy in the $t \approx +0$ day spectrum is indicated with a box, and the blow-up of this absorption is also shown on the left.

the red side of the weak Si II λ6355 could be due to absorption from C II λ6580. The spectrum of SN 2009dc at $t \approx -9$ days is characterized by prominent C II λ6580 absorption, which is comparable in strength to the Si II λ6355. However, there is no evidence that such a strong C II feature is present in the early-time spectra of SN 2011hr, which shows differences from superluminous SNe Ia.

Figure 9 compares the Fe III features of SN 2011hr, SN 1991T, and SN 1999aa. Some Fe lines, identified by modeling performed in Section 4.3, are marked at a velocity of ~12,000 km s^{-1}. The absorption feature shown in the left panel of the plot is a blend of Fe III λ4397, λ4421, and λ4432 and is represented as Fe III (A). The feature shown in the right panel is a multiplet of Fe III λ5082, λ5129, and

Table 4
Distances to SN 2011hr and NGC 2691

Method	Details	Results (Mpc)
Hubble flow[a]	4269 km s^{-1}	59.3 ± 4
Tully–Fisher[b]	*JHK* bands	60.2 ± 10
Phillips relation[c]	$E(B-V) = 0.17$	48.24 ± 8
Phillips relation[d]	$E(B-V) = 0.17$	56.58 ± 4
NIR luminous[e]	*H* band	43.7 ± 5

Notes.
[a] Corrected for Virgo infall, GA, and Shapley (Mould et al. 2000), on the scale of $H_0 = 72$ km s^{-1} Mpc^{-1}.
[b] Mean distance from estimates in the *JHK* bands (Theureau et al. 2007; Tully et al. 2009).
[c] $\Delta m_{15}(B) = 0.92$; Phillips (1993).
[d] Modified Phillips (1993) relation in Figure 13 of Blondin et al. (2012) for 91T-like events.
[e] Weyant et al. (2014).

Table 5
Journal of Spectroscopic Observations of SN 2011hr

Date	MJD (−2,400,000.5)	Epoch[a] (days)	Res. (Å pixel^{-1})	Range (Å)	Slit Width (pixel)	Exp. time (s)	Telescope (+Instrument)
2011 Nov 10	55,875.90	−13.22	1.5	5000–9800	2.8	1200	LJT YFSOC
2011 Nov 10	55,875.92	−13.20	1.8	3340–7680	2.8	1200	LJT YFSOC
2011 Nov 12	55,877.85	−11.27	2.9	3500–8890	4.2	1200	LJT YFSOC
2011 Nov 13	55,878.85	−10.27	1.5	5000–9800	4.2	1200	LJT YFSOC
2011 Nov 13	55,878.87	−10.25	1.8	3340–7680	4.2	1200	LJT YFSOC
2011 Nov 13	55,878.89	−10.23	2.9	3500–8890	4.2	1200	LJT YFSOC
2011 Nov 15	55,880.82	−8.30	2.9	3500–8890	4.2	1200	LJT YFSOC
2011 Nov 19	55,884.84	−4.28	4.1	3580–8565	3.0	3600	XLT BFOSC
2011 Nov 23	55,888.82	−0.30	2.1	5080–7690	3.0	1800	XLT BFOSC
2011 Dec 04	55,899.91	+10.79	2.9	3500–8890	6.4	900	LJT YFSOC
2011 Dec 05	55,900.93	+11.81	2.9	3500–8890	6.4	900	LJT YFSOC
2011 Dec 08	55,903.81	14.69	2.9	3500–8890	6.4	900	LJT YFSOC
2011 Dec 19	55,914.78	25.66	2.9	3500–8890	6.4	900	LJT YFSOC
2011 Dec 23	55,918.57	29.45	4.1	3780–8900	6.0	2700	XLT BFOSC
2012 Jan 25	55,951.76	62.64	2.9	3500–8890	6.4	3000	LJT YFSOC

Note. Journal of spectroscopic observations of SN 2011hr.
[a] Relative to *B*-band maximum on 2011 November 22.3, JD 2,455,889.62.

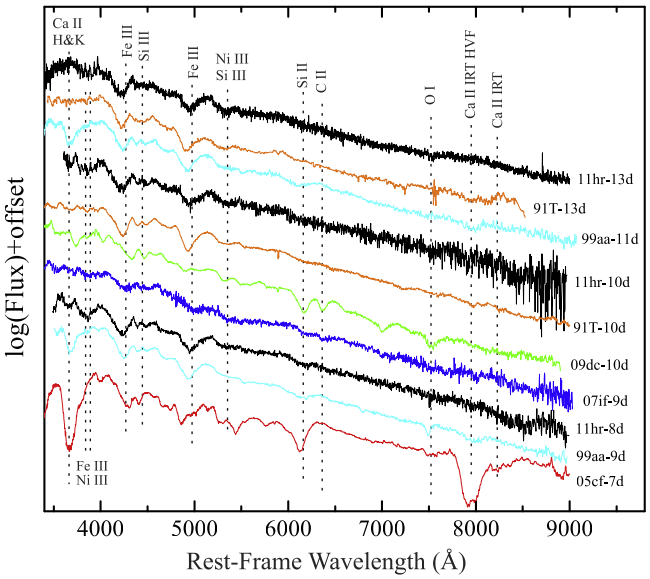

Figure 5. Spectra of SN 2011hr at $t < -7$ days before the *B*-band maximum light. Overplotted are the spectra of SN 1991T (Filippenko et al. 1992b), SN 1999aa (Garavini et al. 2004), and SN 2005cf (Wang et al. 2009b) at comparable phases. The spectra of SN 2011hr are corrected for contaminations of the host galaxy.

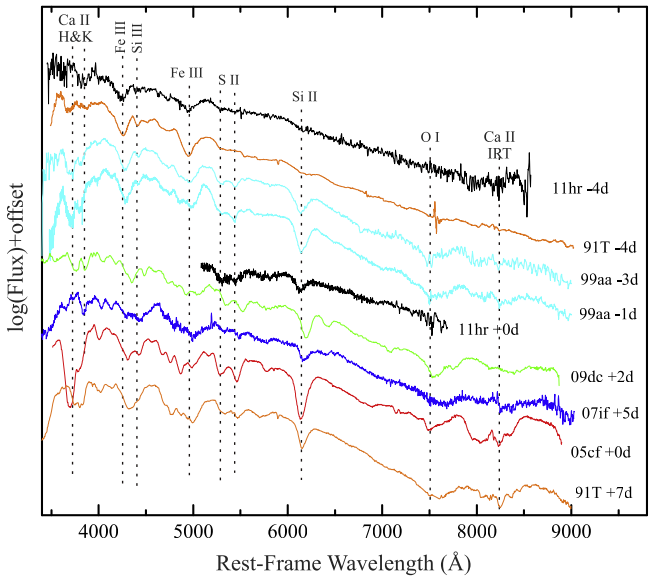

Figure 6. Spectra of SN 2011hr at around maximum light, compared to those of the same SNe Ia as in Figure 5.

λ5158 and is represented as Fe III (B). For the Fe III (A) feature, the three SNe Ia show similarities in the line strength, velocity, and shape at $t \approx -13$ days. For the Fe III (B) feature, SN 2011hr appears weaker than SN 1991T and SN 1999aa on the blue side of the absorption, which is more significant at earlier phases. It is unlikely that this difference is due to the absorption of Fe III λ5082 alone.

3.2.2. The Maximum-light Phase

Figure 6 shows the spectra at around maximum light. At $t \approx -4$ days, the Fe II/Fe III lines appear shallower and wider in SN 2011hr compared to SN 1991T. At this phase, the S II features at ~5300 Å and ~5450 Å start to emerge in the spectra of SN 2011hr and SN 1991T. These lines are useful to follow the shift of the ionization state of IMEs from doubly to singly ionized species. S II features in the spectra of SN 2011hr and SN 1991T are weaker than in SN 1999aa, suggesting a relatively lower ionization state for the latter. Moreover, the Fe III (B) absorption in SN 1999aa may be blended with the Fe II lines, suggesting a lower ionization. In SN 2011hr, the weak absorption near 6150 Å is likely to be Si II λ6355, which may indicate a lower ejecta velocity (see also Figure 10). In other SNe Ia, this Si II feature is stronger at similar phases.

At $t \approx 0$ days, Si II λ6355 finally develops in SN 2011hr, but it does not become as strong as normal SNe Ia. The EW of this line is ~34 Å for SN 2011hr, which is only slightly larger than SN 2007if (i.e., ~25 Å) and smaller than SN 1991T (i.e., ~48 Å), SN 1999aa (i.e., ~56 Å), SN 2005cf (i.e., ~85 Å), and SN 2009dc (i.e., ~51 Å) at similar phases. At this phase, the

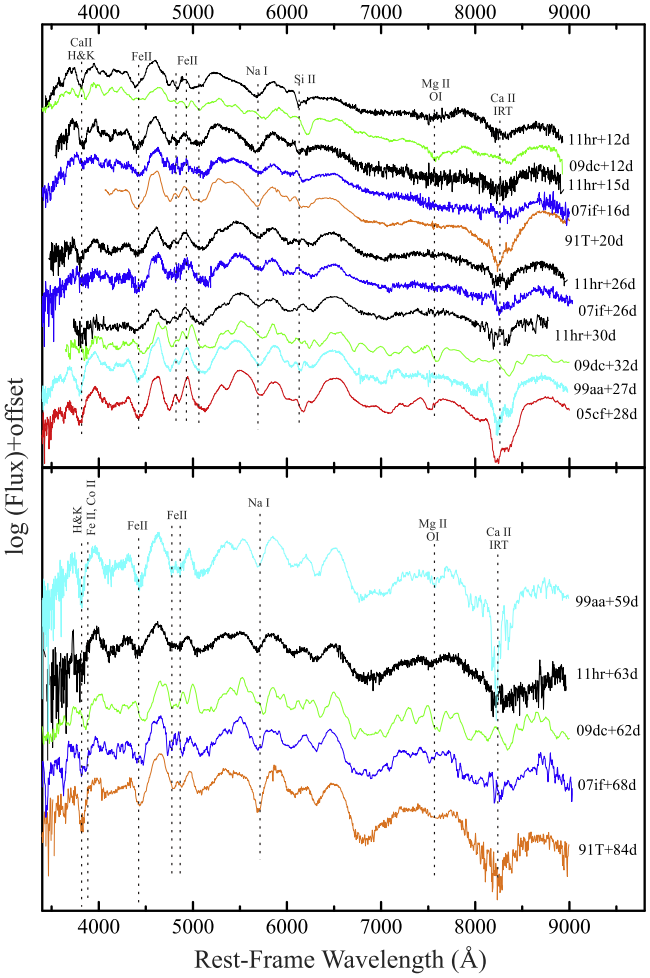

Figure 7. Postmaximum spectra of SN 2011hr, compared to the same SNe as in Figure 5. The spectrum of SN 2007if at $t \approx +68$ is smoothed with a box of 10 (~24 Å). The spectrum of SN 1999aa at $t \approx +59$ days is from Silverman et al. (2012).

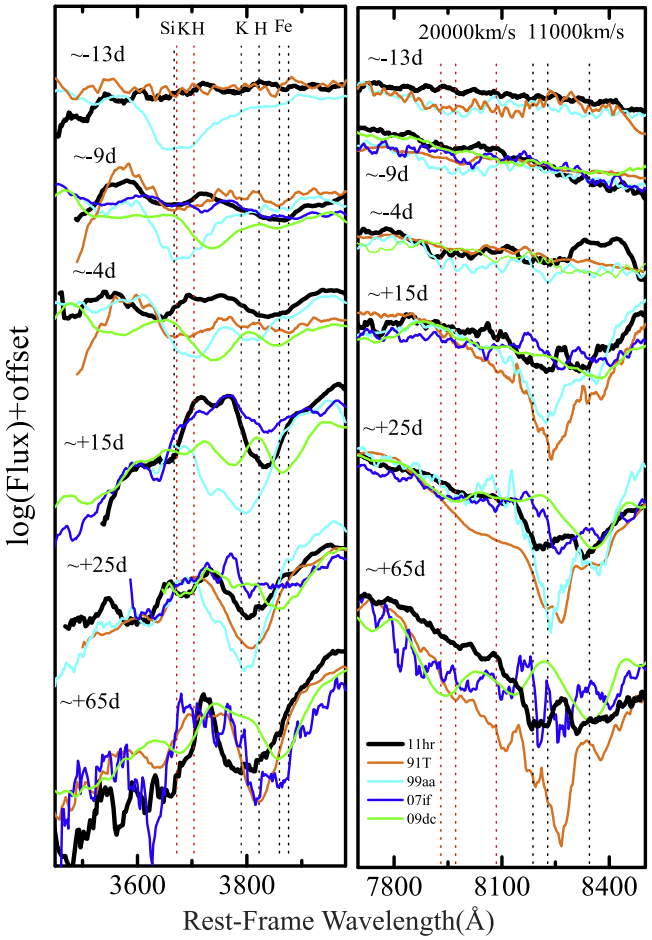

Figure 8. Evolution of the Ca II absorption in the spectra of SN 2011hr, SN 1991T, SN 1999aa, SN 2007if, and SN 2009dc at selected epochs. Left panel: evolution of Ca II H&K and Si II λ3860. Right panel: evolution of Ca II NIR triplet. The positions of Ca II H&K, Si III λ3807, Fe II, and the Ca II NIR triplet lines at different velocities (black dotted lines mark the line positions with $v = 11{,}000$ km s^{-1}, and red dotted lines mark the positions with $v = 20{,}000$ km s^{-1}) are shown to guide the eyes. All spectra are smoothed with a boxcar of 10 (i.e., ~20–30 Å). See Figures 5, 6, and 7 for the exact phase of each spectrum.

"W"-shaped feature of S II lines becomes noticeable in SN 2011hr. The presence of the S II lines indicates that SN 2011hr originated from a thermonuclear runaway. Inspection of Figure 6 reveals that there is no clear signature of O I λ7773 absorption in SN 2011hr and SN 1991T near maximum light. However, this feature becomes obvious in the spectra of other SNe Ia at this phase.

3.2.3. The Postmaximum Phase

The postmaximum spectra of SN 2011hr are compared with those of other SNe Ia in Figure 7. At about 2 weeks after maximum light, the spectrum of SN 2011hr is dominated by lines of iron and sodium, and the Si II λ6355 absorption is still very weak and the O I λ7773 line is almost undetectable at this phase. SN 2007if exhibits similar features in the comparable-phase spectra, while SN 2009dc shows stronger absorptions of Si II λ6355 and O I λ7773 but has lower expansion velocities. Moreover, the Ca II NIR triplets of SN 2011hr, SN 2007if, and SN 2009dc are all weak compared to SN 1991T.

At $t \approx +26$ days, the spectra of SN 2011hr and SN 2007if become more similar. For normal SNe Ia at this phase, the absorption of the Ca II NIR triplet usually evolves to become the strongest feature in the spectra. However, such a line

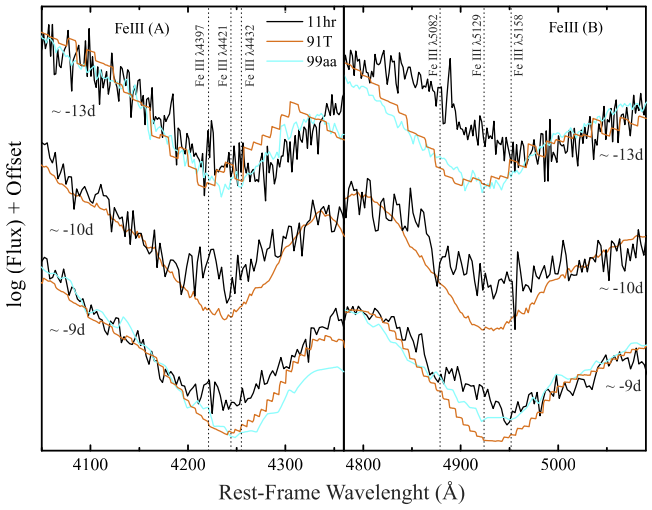

Figure 9. Absorption lines of Fe III in the spectra of SN 2011hr, SN 1991T, and SN 1999aa at early phases. The positions of these lines at a velocity of 12,000 km s^{-1} are marked to guide the eyes.

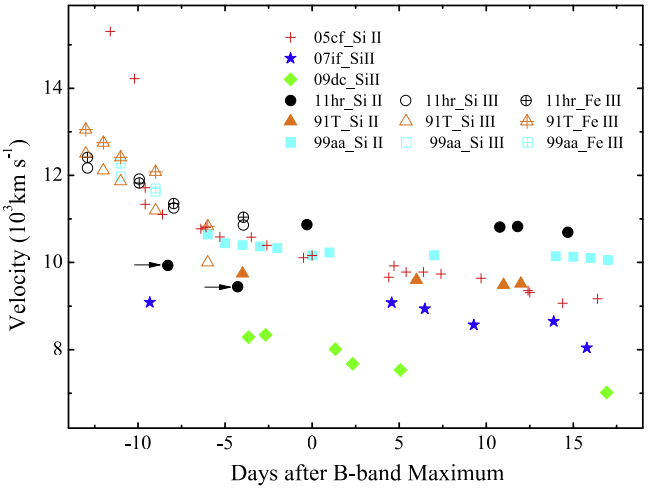

Figure 10. Ejecta velocity evolution of SN 2011hr, SN 1991T, SN 1999aa, SN 2005cf, SN 2007if, and SN 2009dc, as inferred from absorption minima of Si II λ6355, Si III λ4565, and Fe III $\lambda\lambda$4400, 5100 lines.

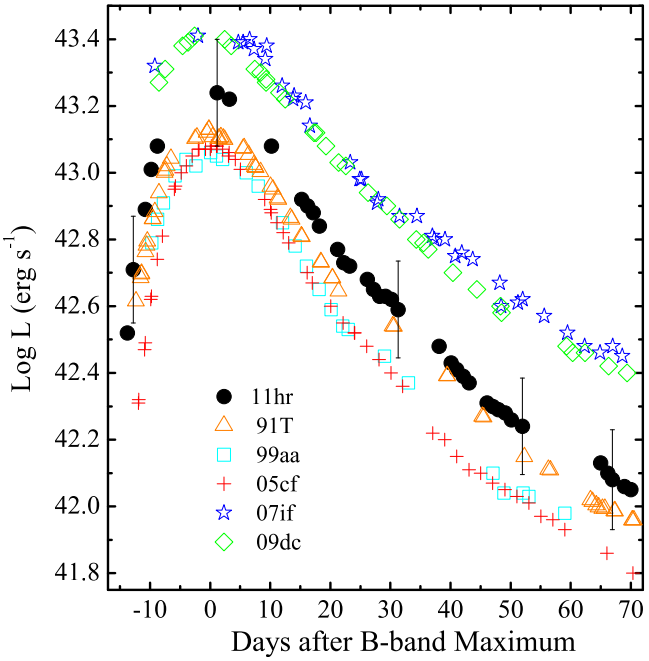

Figure 11. Quasi-bolometric light curves of SN 2011hr derived from the *UBVRI* photometry, compared with those of SN 1991T, SN 1999aa, SN 2005cf, SN 2007if, and SN 2009dc.

feature is still rather weak in SN 2011hr, SN 2007if, and SN 2009dc. At this phase, SN 1991T and SN 1999aa show absorption of the Ca II NIR triplet that is as strong as that seen in normal SNe Ia. At 2–3 months later, absorption of the Ca II NIR triplet grows in strength in SN 2011hr, SN 2007if, and SN 2009dc, but it is still significantly weaker compared to that seen in SN 1991T and SN 1999aa. The postmaximum spectra of SN 2011hr show distinct behavior relative to normal SNe Ia but are overall very similar to those of SN 2007if, including the velocity and strength of different species.

3.3. Velocities of the Ejecta

Figure 10 shows the ejecta velocity of SN 2011hr measured via the absorption feature of Fe III before maximum light and Si II λ6355 after the peak. The absorption near 4300 and 5000 Å is produced by blends of Fe III lines, with rest wavelengths marked in Figure 5. A mean wavelength is adopted for each feature in the velocity estimation. The position of the blueshifted absorption minimum was measured using both the Gaussian fit and the direct measurement of the center of the absorption, and the results are averaged. The results for the two groups of Fe III lines are also averaged in this figure. The first two points of Si II λ6355 of SN 2011hr are derived from center of the minor absorption around 6200 Å, which are $\sim$1000 km s^{-1} lower than the measurement at $t \approx +0$ days. This might suggest that this feature is not due to Si II λ6355, but it is more likely that the Si II line grows in strength and velocity owing to recombination and that its optical depth at higher velocities increases with time in spite of decreasing density. The Si II λ6355 velocity near maximum light is estimated as $v = 10.88 \pm 0.15 \times 10^3$ km s^{-1} for SN 2011hr, which is closer to that of SN 1991T and SN 1999aa. SN 2007if and SN 2009dc have lower velocities, which suggests that they may have different ejecta structures.

The velocity gradient of SN 2011hr, derived from absorption of Si II λ6355 during the period from $t \approx +0$ to $t \approx +15$ days, is 9 ± 10 km s^{-1}day^{-1}. This is comparable to that of SN 1999aa, SN 1991T, and SN 2007if, which places SN 2011hr in the low-velocity gradient (LVG) category of SNe Ia according to the classification scheme of Benetti (2005). After maximum light, SN 2011hr shows a higher Si II velocity relative to the comparison SNe Ia, indicating that the inner boundary of the Si shell is located at higher velocities. If the inner layers are dominated by Fe-group elements (Mazzali et al. 2007), this implies that SN 2011hr produced more ^{56}Ni than the normal SNe Ia.

4. DISCUSSION

4.1. Quasi-bolometric Luminosity

Figure 11 displays the quasi-bolometric light curves of SN 2011hr derived from the *UBVRI* photometry, compared to those of SN 1991T (Sasdelli et al. 2014), SN 1999aa (Jha et al. 2006), SN 2005cf (Wang et al. 2009b), SN 2007if (Scalzo et al. 2010), and SN 2009dc (Taubenberger et al. 2010). Note that the brightness of SN 2011hr is located at the middle of SN 1991T/SN 1999aa and SN 2007if/SN 2009dc. However, the bolometric light curve of SN 2011hr is similar to that of SN 1991T and SN 1999aa in morphology. The superluminous SN 2007if and SN 2009dc show apparently wider light curves. These suggest that SN 2011hr may have a somewhat different explosion mechanism from these superluminous SNe Ia, although it shares some spectroscopic properties with SN 2007if.

To estimate the ^{56}Ni mass synthesized in the explosion of SN 2011hr, we need to calculate its generic bolometric luminosity at maximum light. The UV emission of SN 2011hr was estimated by assuming that it has a similar ratio of UV to *B*-band flux as the well-sampled 99aa-like event iPTF14bdn (Smitka et al. 2015), while the NIR contribution was extrapolated based on its *J* & *H*-band photometry published by Weyant et al. (2014). The peak "*uvoir*" bolometric luminosity is thus estimated to be $(2.30 \pm 0.90) \times 10^{43}$ erg s^{-1}. Applying a t^2 model to the observed *R*-band light curve yields an explosion time of MJD = 55,869.7 ± 1.0 and a rise time of 19.4 ± 1.0 days in

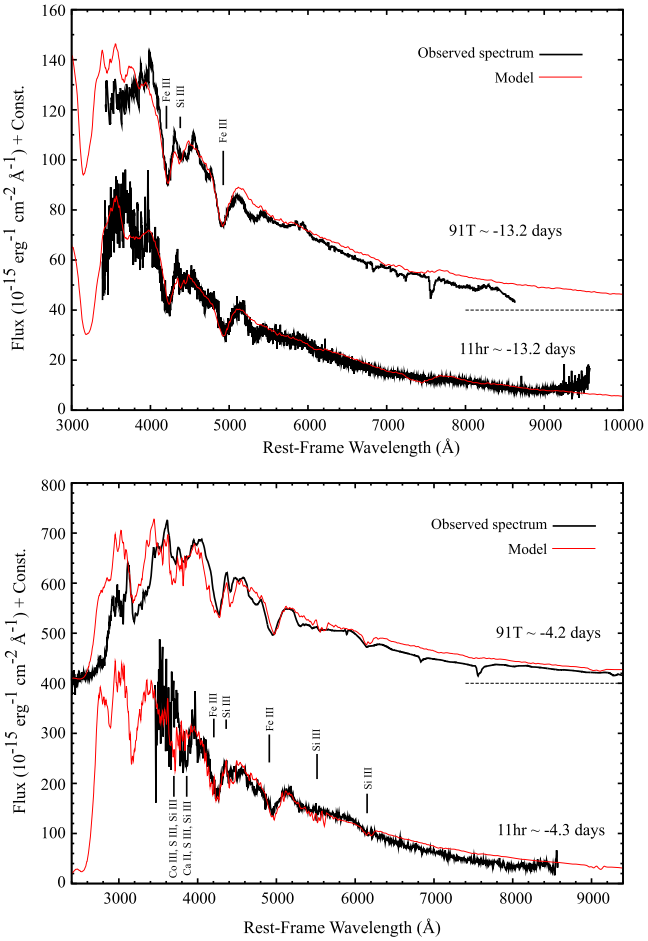

Figure 12. Synthetic spectra are compared with the observed spectra of SN 2011hr at −13.2 and −4.3 days. At the top of each panel, the model and the observed spectrum of SN 1991T at the same epoch from Sasdelli et al. (2014) are shown for comparison. To allow the comparison between these two SNe, the flux of SN 2011hr has been scaled by putting it at the same distance as SN 1991T. The spectra are in rest frame and corrected for reddening by the amount assumed during the modeling.

B band, which is close to the estimate derived from the spectral modeling (i.e., ∼20 days in the *B* band; see discussions in Section 4.1). Considering the UV contribution, the bolometric curve of SN 2011hr reaches its peak at about 1.4 days earlier than in *B* band; a rise time of 18.0 ± 1.0 days is thus adopted for SN 2011hr in the following analysis. Based on these parameters, we estimate that the ^{56}Ni mass synthesized in the explosion of SN 2011hr is $M(^{56}\mathrm{Ni}) = 1.11 \pm 0.43\ M_{\odot}$ according to the Arnett law (Arnett 1982; Stritzinger & Leibundgut 2005). This value is larger than that obtained for SN 1991T ($M(^{56}\mathrm{Ni}) = 0.82\ M_{\odot}$), SN 1999aa ($M(^{56}\mathrm{Ni}) = 0.72\ M_{\odot}$), and SN 2005cf ($M(^{56}\mathrm{Ni}) = 0.75\ M_{\odot}$). The ^{56}Ni masses inferred for SN 2007if and SN 2009dc (with a similar method) are much larger, which are close to 2.0 $M_{\odot}$. An accurate determination of the ^{56}Ni mass could be also obtained using nebular spectra (Mazzali et al. 2007), but no late-time spectra are available for SN 2011hr.

4.2. Explosion Models

Our observations indicate that SN 2011hr is an overluminous SN Ia. Both the SC-mass and the Chandrasekhar-mass scenario have been proposed to explain observational features of overluminous SNe Ia. Yoon & Langer (2005) suggested that the WDs may accrete mass from a nondegenerate or another WD companion star and grow in mass to values exceeding the Chandrasekhar-mass limit (which can reach a mass of $\gtrsim 2.0\ M_{\odot}$ if the WD is in differential rotation). Thermonuclear explosions of rapidly rotating WDs have been suggested to account for production of superluminous SNe Ia in terms of both burning products and explosion kinematics by Pfannes et al. (2010a, 2010b). Also, they find that a rotating WD that detonates has an ejecta velocity compatible with that of a normal SN Ia. Meanwhile, Pfannes et al. (2010a, 2010b) also showed that a significant amount of IMEs are produced for rotating SC-mass WDs. Inspection of Figure 6 reveals that SN 2011hr has rather weak absorption features of Si II, Ca II, and O I, unlike the 91T-like and normal SNe Ia. These results indicate that the IMEs (especially Ca) are apparently less abundant in SN 2011hr, which seems to be inconsistent with the predictions of rotating SC-mass WDs (see Pfannes et al. 2010a, 2010b).

Alternatively, SN 2011hr may be an energetic explosion of a Chandrasekhar-mass WD. For instance, the Chandrasekhar-mass model with a high kinetic energy in Iwamoto et al. (1999) may be a good candidate for producing overluminous SNe Ia, which will be addressed in Section 4.3. The gravitationally confined detonation (GCD) of near-Chandrasekhar-mass WDs may be an alternative scenario to explain the overluminous SNe Ia. The GCD model has been studied by different groups (e.g., Plewa et al. 2004, 2007; Meakin et al. 2009; Jordan et al. 2012). On one hand, it has been shown that the GCD model may provide explanations for overluminous SN 1991T-like events because it can produce a large mass of ^{56}Ni that can even exceed 1.0 $M_{\odot}$. On the other hand, GCD models naturally produce chemically mixed compositions and thus are proposed to explain the high-velocity Fe-group elements observed in early-time spectra of some overluminous 91T-like SNe. Unfortunately, to date, no detailed radiative transfer calculations have yet been performed to compare with the observations of overluminous SNe Ia.

Finally, we point out that the absence of C and O lines in the early-time spectra of SN 2011hr suggests that SN 2011hr is unlikely to be the result of the merger of two WDs (i.e., the so-called violent merger model within the double-degenerate scenario).

4.3. Abundance Tomography of SN 2011hr

To set further constraints on the possible progenitor scenario, we modeled the early spectra of SN 2011hr using a well-tested Monte Carlo code that was initially developed by Mazzali & Lucy (1993) and later improved by Lucy (1999) and Mazzali (2000) by including the photon branching. The code assumes a photosphere with a scaled blackbody emission. This approximation is valid when the inner part of the ejecta that encloses most of the radioactive materials is optically thick. To model the spectra, we adopt a technique called "abundance tomography" (Stehle et al. 2005; Mazzali et al. 2008; Tanaka et al. 2011; Ashall et al. 2014; Sasdelli et al. 2014). As shown in previous sections, there are some uncertainties in determinations of the distance and host-galaxy reddening for SN 2011hr. A higher luminosity may require an SC-mass progenitor, e.g., $M(^{56}\mathrm{Ni}) = 1.61\ M_{\odot}$ if $E(B-V) = 0.27$ and $D = 66$ Mpc. We want to investigate whether a Chandrasekhar-mass scenario is still viable for SN 2011hr, or whether it can only be

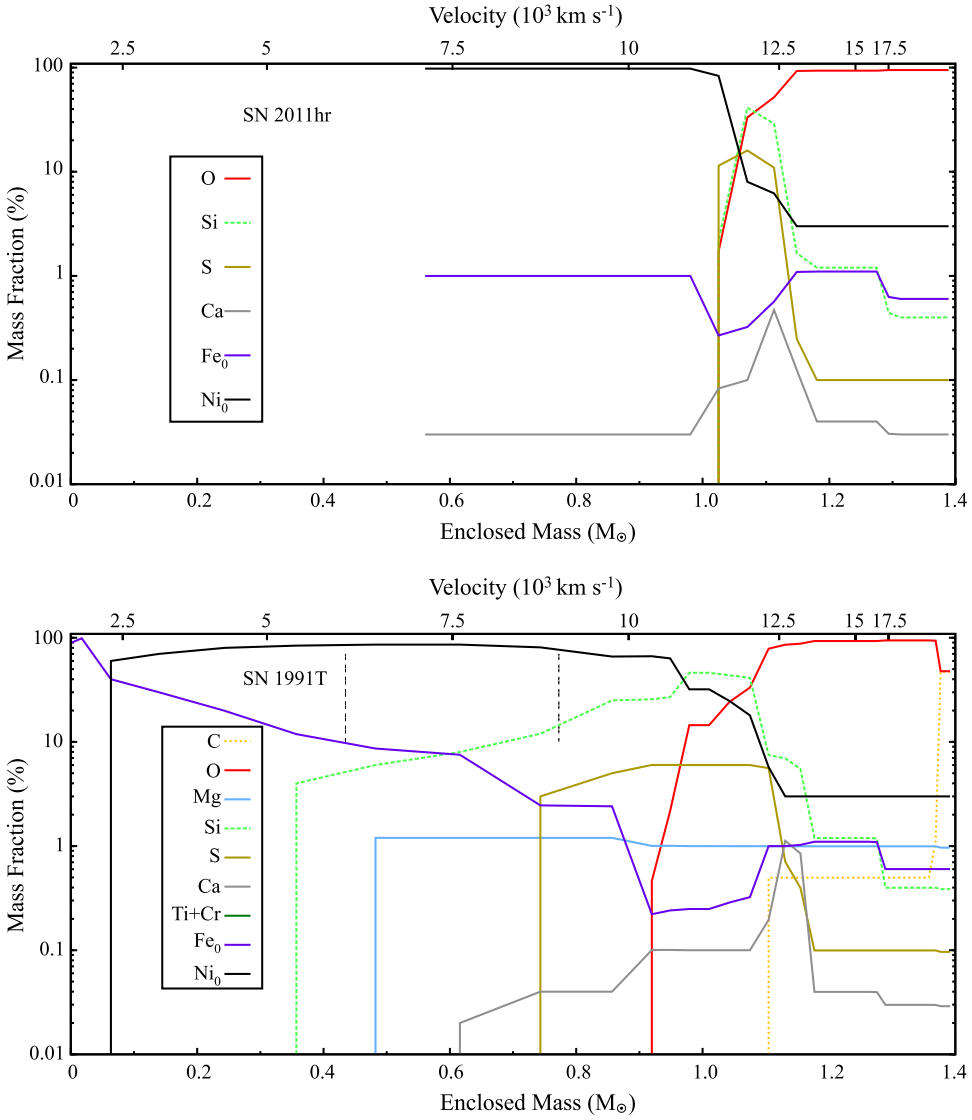

Figure 13. Abundance distribution of the outer ejecta inferred for SN 2011hr and SN 1991T. SN 2011hr (top panel) has a thinner layer of IMEs above a large amount of ^{56}Ni. Only the outer layers can be probed with the photospheric method adopted here. The abundances of SN 1991T (bottom panel) are taken from Figure 5 of Sasdelli et al. (2014).

explained with an SC-mass model. For our investigation, we use the density profile of the energetic WDD3 model from Iwamoto et al. (1999). This should be a good choice for SN 2011hr, which shows lines with relatively higher velocities.

We fit the luminosity of SN 2011hr from spectral modeling. This is an independent estimate of the distance and the extinction. We follow the same method as that described in Sasdelli et al. (2014) to study the luminosity of SN 1991T, which is an ideal SN for a comparative study with SN 2011hr. Similarly to SN 1991T, the time at which the recombination from Si III into Si II happens can place a tight constraint on the luminosity. For SN 2011hr, this transition happens at a couple of days later than SN 1991T. Figure 12 displays the comparison of the modeled spectra of SN 2011hr at $t \approx -13$ days and -4 days, respectively. The observed and modeled spectra of SN 1991T are also shown as references. The distance adopted for SN 2011hr is $D = 60$ Mpc (i.e., $m - M = 33.89$). In addition to the Milky Way reddening of $E(B-V) = 0.02$, we use a reddening $E(B-V) = 0.15$ for the host galaxy. A larger reddening is disfavored by the synthetic color from the model spectrum.

Compared to SN 1991T, the Fe III features at 4200 and 4900 Å are less pronounced in SN 2011hr. The modeling analysis shows that this can be explained with an ionization effect, as a consequence of the fact that the temperature of SN 2011hr is higher than that of SN 1991T. The Si II line at 6100 Å first appears at around the B-band maximum light, ~4 days later than in SN 1991T. Again, this can also be due to an ionization effect caused by the higher luminosity of SN 2011hr. On the other hand, the Si III λ4450 line is weaker than in SN 1991T despite a larger fraction of Si III because of a lower Si abundance. Si is the dominant element only within 11,500 and 12,000 km s^{-1}. SN 2011hr has an abundance profile qualitatively similar to SN 1991T, but likely representing a more extreme case (i.e., Figure 13). The interface between the ^{56}Ni-dominated interior and the layer dominated by IMEs is thinner in SN 2011hr compared to that seen in SN 1991T. The ^{56}Ni fraction exceeds 90% up to velocities as high as ~11,500 km s^{-1}. This matches the lowest velocities of Si II

measured in the spectra. The layer dominated by Si and other IMEs is also thinner than in SN 1991T, and their total mass is just 0.07 $M_{\odot}$, while in SN 1991T the IME mass is 0.18 $M_{\odot}$ (Sasdelli et al. 2014). We could recap the properties of SN 2011hr as "more 91T-like than SN 1991T itself."

The modeling result shows that the luminosity of SN 2011hr is higher than SN 1991T by about 20%. This requires a ^{56}Ni mass of about 0.94 $M_{\odot}$. The luminosity of SN 2011hr is at the brightest end of SNe Ia, which requires a large amount of ^{56}Ni, but this is balanced by a lower mass of IMEs. The model does not require a mass larger than the Chandrasekhar mass, and instead it suggests that a scenario with an efficiently burned Chandrasekhar mass is also possible to produce such an overluminous SN Ia.

5. CONCLUSION

We have presented extensive observations and studies of the luminous (e.g., $M_{\max}(B) = -19.84 \pm 0.40$ mag), spectroscopically peculiar SN Ia SN 2011hr. It exhibits light-curve evolution that is similar to SN 1991T, with a postmaximum decline rate $\Delta m_{15}(B) = 0.92 \pm 0.03$ mag. The spectra of SN 2011hr are characterized by strong Fe-group lines and weak absorptions of IMEs, showing close resemblances to that of SN 2007if at all phases. Note, however, that the absence of C II absorption in the early-time spectra of SN 2011hr suggests that there should be differences between these two SNe Ia. Moreover, SN 2011hr has narrower light-curve peaks and its light curves decline more rapidly at late phases compared to SN 2007if. Overall, SN 2011hr shows more similarities with SN 1991T in morphology of the light curves, while it bears more common features with SN 2007if in the spectral evolution.

Computing the detailed abundance distribution of the IMEs and iron-group elements helps further reveal the nature of this peculiar SN Ia. Mapping the abundances in the outer ejecta with the abundance tomography method, we found that a lower mass of IMEs (i.e., 0.07 $M_{\odot}$) and a larger mass of ^{56}Ni (i.e., ~0.94 $M_{\odot}$ by spectral modeling or ~1.11 $M_{\odot}$ by Arnett law) can be inferred for SN 2011hr. The corresponding values inferred for SN 1991T are ~0.18 $M_{\odot}$ for IMEs and ~0.78 $M_{\odot}$ for ^{56}Ni. Our models suggest that a very efficiently burned Chandrasekhar-mass progenitor is the favored scenario for this overluminous SN Ia. The weaker absorptions of the IMEs might indicate a lower abundance of these elements in the outer ejecta. Nevertheless, the presence of similar features in SN 2011hr and SN 2007if may indicate that SN 2011hr represents a transitional object linking 91T-like SNe Ia to some superluminous SNe Ia.

We acknowledge the support of the staff of the Li-Jiang 2.4 m telescope (LJT), Xing-Long 2.16 m telescope, and Tsinghua-NAOC 0.8 m telescope (TNT). Funding for the LJT has been provided by the Chinese Academy of Sciences (CAS) and the People's Government of Yunnan Province. The TNT is owned by Tsinghua University and jointly operated by the National Astronomical Observatory (NAOC) of the CAS. Financial support for this work has been provided by the National Science Foundation of China (NSFC, grants 11403096, 11178003, 11325313, 11133006, 11361140347, 11203034, 11473063, 11322327, 11103072, 11203078, 11303085, 11203070 and 11103078); the Major State Basic Research Development Program (2013CB834903); the Strategic Priority Research Program "The Emergence of Cosmological Structures" of the CAS (grant No. XDB09000000); the Key Research Program of the CAS (Grant NO. KJZD-EW-M06); the Western Light Youth Project; the Youth Innovation Promotion Association of the CAS; the Open Project Program of the Key Laboratory of Optical Astronomy, NAOC, CAS; and the key Laboratory for Research in Galaxies and Cosmology of the CAS.

REFERENCES

Altavilla, G., Fiorentino, G., Marconi, G., et al. 2004, MNRAS, 349, 1344
Arnett, W. D. 1982, ApJ, 253, 785
Ashall, C., Mazzali, P., Bersier, D., et al. 2014, MNRAS, 445, 4427
Barbon, R., Benetti, S., Rosino, L., Cappellaro, E., & Turatto, M. 1990, A&A, 237, 79
Barone-Nugent, R. L., Lidman, C., Wyithe, J. S. B., et al. 2012, MNRAS, 425, 1007
Benetti, S. 2005, ApJ, 623, 1011
Bessell, M. S. 1990, PASP, 102, 1181
Blondin, S., Matheson, T., Kirshner, R. P., et al. 2012, AJ, 143, 126
Blondin, S., & Tonry, J. L. 2007, ApJ, 666, 1024
Branch, D., Dang, L. C., & Baron, E. 2009, PASP, 121, 238
Branch, D., Baron, E., Hall, N., et al. 2005, PASP, 117, 545
Branch, D., Dang, L. C., Hall, N., et al. 2006, PASP, 118, 560
Brown, P. J., Kuin, P., Scalzo, R., et al. 2014, ApJ, 787, 29
Cardelli, J. A., Clayton, G. C., & Mathis, J. S. 1989, ApJ, 345, 245
Childress, M. J., Filippenko, A. V., Ganeshalingam, M., et al. 2014, MNRAS, 437, 338
Childress, M. J., Scalzo, R. A., Sim, S., et al. 2013, ApJ, 770, 29
Cousins, A. 1981, SAAOC, 6, 4
Dilday, B., Howell, D. A., Cenko, S. B., et al. 2012, Sci, 337, 942
Fan, Y. F., Bai, J. M., Zhang, J. J., et al. 2015, RAA, 15, 918
Filippenko, A. V. 1997, ARA&A, 35, 309
Filippenko, A. V., Richmond, M. W., Branch, D., et al. 1992a, AJ, 104, 1543
Filippenko, A. V., Richmond, M. W., Michael, W., et al. 1992b, ApJL, 384, L15
Fisher, A., Branch, D., Hatano, K., & Baron, E. 1999, MNRAS, 304, 67
Fitzpatrick, E. L., & Massa, D. 2007, ApJ, 663, 320
Foley, R. J., Challis, P. J., Chornock, R., et al. 2013, ApJ, 767, 57
Garavini, G., Folatelli, G., Goobar, A., et al. 2004, AJ, 128, 387
Gibson, B. K., & Stetson, P. B. 2001, ApJL, 547, L103
Goldhaber, G., Groom, D. E., Kim, A., et al. 2001, ApJ, 558, 359
Guy, J., Astier, P., Nobili, S., et al. 2005, A&A, 443, 781
Hachinger, S., Mazzali, P. A., Taubenberger, S., et al. 2012, MNRAS, 427, 2057
Hamuy, M., Phillips, M. M., Suntzeff, N. B., et al. 1996, AJ, 12, 2438
Hicken, M., Garnavich, P. M., Prieto, J. L., et al. 2007, ApJL, 669, L17
Hicken, M., Wood-Vasey, W. M., Blondin, S., et al. 2009, ApJ, 700, 1097
Hillebrandt, W., Sim, S. A., & Röpke, F. K. 2007, A&A, 465, 17
Howell, D., Sullivan, M., Nugent, P. E., et al. 2006, Natur, 443, 308
Huang, F., Li, J. Z., Wang, X. F., et al. 2012, RAA, 11, 1585
Iwamoto, K., Brachwitz, F., Nomoto, K., et al. 1999, ApJS, 125, 439
Jha, S., Krishner, R. P., Challis, P., et al. 2006, AJ, 131, 527
Johnson, H., Iriarte, B., Mitchell, R., & Wisniewskj, W. 1966, CoLPL, 4, 99
Jordan, G. C., IV, Graziani, C., Fisher, R. T., et al. 2012, ApJ, 759, 53
Krisciunas, K., Phillips, M. M., & Suntzeff, N. B. 2004, ApJL, 602, L81
Landolt, A. V. 1992, AJ, 104, 340
Li, W., Filippenko, A., Ryan, C., et al. 2003, PASP, 115, 453
Lira, P., Suntzeff, N. B., Phillips, M. M., et al. 1998, AJ, 115, 234
Lucy, L. B. 1999, A&A, 345, 211
Maeda, K., Leloudas, G., Taubenberger, S., et al. 2011, MNRAS, 413, 3075
Maeda, K., Benetti, S., Stritzinger, M., et al. 2010, Natur, 466, 82
Maoz, D., Mannucci, F., & Nelemans, G. 2014, ARA&A, 52, 107
Marion, G. H., Vinko, J., Wheeler, J. C., et al. 2013, ApJ, 777, 40
Maund, J., Hörflich, P., Patat, F., et al. 2010, ApJL, 725, L167
Mazzali, P. A. 2000, A&A, 363, 705
Mazzali, P. A., Benetti, S., Altavilla, G., et al. 2005, ApJL, 623, L37
Mazzali, P. A., Danziger, I. J., & Turatto, M. 1995, A&A, 297, 509
Mazzali, P. A., & Lucy, L. B. 1993, A&A, 279, 447
Mazzali, P. A., Röpke, F. K., Benetti, S., & Hillebrandt, W. 2007, Sci, 315, 825
Mazzali, P. A., Sauer, D. N., Pastorello, A., Benetti, S., & Hillebrandt, W. 2008, MNRAS, 386, 1897
Meakin, C. A., Seitenzahl, I., Townsley, D., et al. 2009, ApJ, 693, 1188
Meikle, W. P. S. 2000, MNRAS, 314, 782

Mould, J. R., Huchra, J. P., Freedman, W.L., et al. 2000, ApJ, 529, 786
Nayak, I., Cenko, S. B., & Filippenko, A. V. 2011, CEBT, 2837
O'Donnell, J. E. 1994, ApJ, 422, 158
Perlmutter, S., Aldering, G., Goldhaber, G., et al. 1999, ApJ, 517, 565
Pfannes, J. M. M., Niemeyer, J. C., & Schmidt, W. 2010a, A&A, 509, 75
Pfannes, J. M. M., Niemeyer, J. C., Schmidt, W., & Klingenberg, C. 2010b, A&A, 509, 74
Phillips, M. 1993, ApJL, 413, L105
Phillips, M., Lira, R., Suntzeff, N. B., et al. 1999, AJ, 118, 1766
Phillips, M., Simon, J., Morrell, N., et al. 2013, ApJ, 779, 38
Phillips, M., Wells, L. A., Suntzeff, N. B., et al. 1992, AJ, 103, 1632
Plewa, T., Calder, A. C., Lamb, D. Q., et al. 2004, ApJL, 612, L37
Plewa, T. 2007, ApJ, 657, 942
Poznanski, D., Ganeshalingam, M., Silverman, J. M., & Filippenko, A. V. 2011, MNRAS, 415, L81
Riess, A., Filippenko, A. V., Challis, P., et al. 1998, AJ, 116, 1009
Riess, A., Press, W., & Kirshner, R. 1996, ApJ, 473, 88
Ruiz-Lapuente, P., Cappellaro, E., Turatto, M., et al. 1992, ApJL, 387, L33
Sasdelli, M., Mazzali, P. A., Pian, E., et al. 2014, MNRAS, 445, 711
Scalzo, R., Aldering, G., Antilogus, P., et al. 2010, ApJ, 713, 1073
Schlegel, D., Finkbeiner, D., & Davis, M. 1998, ApJ, 500, 525
Schmidt, B., Suntzeff, N., Phillips, M., et al. 1998, ApJ, 507, 46
Silverman, J., Foley, R. J., Filippenko, A. V., et al. 2012, MNRAS, 425, 1789
Silverman, J., Ganeshalingam, M., Li, W., et al. 2011, MNRAS, 410, 585
Sim, S., Sauer, D. N., Röpke, F. K., & Hillebrandt, W. 2007, MNRAS, 378, 2
Smitka, M. T., Brown, P. J., Suntzeff, N. B., et al. 2015, ApJ, 813, 30
Stehle, M., Mazzali, P. A., Benetti, S., & Hillebrandt, W. 2005, MNRAS, 360, 1231
Stetson, P. 1987, PASP, 99, 191
Stritzinger, M., & Leibundgut, B. 2005, A&A, 431, 423
Suntzeff, N. 1996, in Supernovae and Supernova Remnants, ed. R. McCray, & Z. Wang (Cambridge: Cambridge Univ. Press), 41
Tanaka, M., Mazzali, P. A., Stanishev, V., et al. 2011, MNRAS, 410, 1725
Taubenberger, S., Benetti, S., Childress, M., et al. 2010, MNRAS, 412, 2735
Theureau, G., Hanski, M. O., Coudreau, N., et al. 2007, A&A, 465, 71
Tully, R. B., Rizzi, L., Shaya, E., et al. 2009, AJ, 138, 323
Turatto, M., Benetti, S., & Cappellaro, E. 2003, in From Twilight to Highlight: The Physics of Supernovae, ed. B. Leibundgut, & W. Hillebrandt (Berlin: Springer), 200
Wang, X., Filippenko, A. V., Ganeshalingam, M., et al. 2009a, ApJL, 699, L139
Wang, X., Li, W., Filippenko, A., et al. 2009b, ApJ, 697, 380
Wang, X., Li, W., Filippenko, A. V., et al. 2008, ApJ, 675, 626
Wang, X., Wang, L., Filippenko, A., et al. 2013, Sci, 340, 170
Wang, X. F., Wang, L. F., Filippenko, A. V., et al. 2012, ApJ, 749, 126
Weyant, A., Michael, W., Allen, L., et al. 2014, ApJ, 784, 105
Yoon, S. C., & Langer, N. 2005, A&A, 435, 967
Zhang, J. J., Wang, X. F., Bai, J. M., et al. 2014, AJ, 148, 1
Zhang, T. M., Zhang, J. J., & Wang, X. F. 2011, CEBT, 2901